AIAA JOURNAL
Vol. 49, No. 4, April 2011

Optimization of Composite Structures to Delay Mode Jump Instabilities

Andrea A. Faggiani* and Brian G. Falzon†
Monash University, Clayton, Victoria 3800, Australia
and
Dominik Brunner‡
ETH Swiss Federal Institute of Technology, CH-8092 Zürich, Switzerland

DOI: 10.2514/1.J050590

Numerous studies have shown that postbuckling stiffened panels may undergo abrupt changes in buckled mode shape when loaded in uniaxial compression. This phenomenon is often referred to as a mode jump or secondary instability. The resulting sudden release of stored energy may initiate damage in vulnerable regions within a structure, for example, at the skin-stiffener interface of a stiffened composite panel. Current design practice is to remove a mode jump by increasing the skin thickness of the postbuckling region. A layup optimization methodology, based on a genetic algorithm, is presented, which delays the onset of secondary instabilities in a composite structure while maintaining a constant weight and subject to a number of design constraints. A finite element model was developed of a stiffened panel's skin bay, which exhibited secondary instabilities. An automated numerical routine extracted information directly from the finite element displacement results to detect the onset of initial buckling and secondary instabilities. This routine was linked to the genetic algorithm to find a revised layup for the skin bay, within appropriate design constraints, to delay the onset of secondary instabilities. The layup optimization methodology, resulted in a panel that had a higher buckling load, prebuckling stiffness, and secondary instability load than the baseline design.

Nomenclature

c	=	damping factor
$E_{11\text{compression}}$	=	longitudinal compressive modulus
$E_{11\text{tension}}$	=	longitudinal tensile modulus
$E_{22\text{compression}}$	=	transverse compressive modulus
$E_{22\text{tension}}$	=	transverse tensile modulus
$\mathbf{f}_{\text{damp}}$	=	pseudodamping force vector
$\mathbf{f}_{\text{ext}}$	=	external force vector
$\mathbf{f}_{\text{int}}$	=	internal force vector
G	=	in-plane shear modulus
$\mathbf{M}$	=	consistent mass matrix
n	=	number of sampling points
$\mathbf{r}$	=	residual force vector
S	=	in-plane shear strength
T	=	ply thickness
t	=	pseudotime
u_1, u_2	=	in-plane displacements
u_3	=	out-of-plane displacements
X_c	=	longitudinal compressive strength
X_t	=	longitudinal tensile strength
Y_c	=	transverse compressive strength
Y_t	=	transverse tensile strength
Δt	=	pseudotime increment
λ	=	load multiplier
λ_i	=	ith eigenvalue
ν	=	Poisson's ratio
φ_i	=	eigenvector corresponding to ith eigenvalue

Received 4 April 2010; revision received 27 October 2010; accepted for publication 4 December 2010.

*Research Fellow, Department of Mechanical and Aerospace Engineering, Building 31, Clayton Campus, Wellington Road.

†Professor of Aerospace Engineering, Department of Mechanical and Aerospace Engineering, Building 31, Clayton Campus, Wellington Road (Corresponding Author).

‡Graduate Student, Department of Mechanical and Process Engineering.

I. Introduction

A SUBSTANTIAL body of experimental and theoretical investigations [1–5] has shown that suitably-supported thin-skinned panels loaded in compression may undergo a secondary instability in their postbuckled state. This phenomenon is also referred to as a mode jump or a mode switch and tends to happen abruptly. It is the dynamic nature of this phenomenon which has given cause for concern in the design of thin-skinned composite panels [6] and recent experimental evidence has indicated that secondary instabilities may cause structural failure in adhesively-bonded stiffened composite panels [7,8]. The impetus towards the development of lighter aircraft structures has encouraged the design of postbuckling structures, where certain parts of the structure may be allowed to buckle below the design limit load but usually above the operational design load. Added to this, is the move towards the use of more adhesive bonding over mechanical fasteners. This is especially the case for composite aerostructures where the use of mechanical fasteners presents its own set of potential problems not commonly associated with joining metallic subcomponents. Under such conditions, the possibility of a composite structure experiencing a secondary instability during its operational life cannot be overlooked.

This paper builds on work by the authors, reported in an earlier paper [7], where an optimization strategy was presented for delaying the onset of structural failure, through skin-stiffener debonding, in a postbuckling stiffened composite panel. This was achieved by minimizing the total accumulated damage at the skin-stiffener interfaces. A genetic algorithm (GA) coupled with a commercial finite element (FE) solver, ABAQUS [9] was used for the optimization. GAs have found dependable use in stacking sequence optimization problems. First developed by Holland [10], GAs mimic the genetic operators which exist in natural evolution to evolve an initial, random population towards an optimum solution. Considerable work has been conducted in the field of GAs to optimize various composite structures for different objectives and constraints [7,11–20]. A consequence of the optimized result in [7] was that the secondary instability, observed in the benchmark panel, was delayed.

Table 1 Material properties for T800/924C unidirectional composite

Property	Value
$E_{11\text{tension}}$	162 GPa
$E_{11\text{compression}}$	145 GPa
$E_{22\text{tension}}$	9.2 GPa
$E_{22\text{compression}}$	9.5 GPa
G	5.0 GPa
v	0.3
T	0.125 mm

This was an encouraging result which lent further support to the hypothesis that secondary instabilities may promote structural failure. On this basis it is reasonable to assume that designing a structure which avoided a secondary instability would mitigate the possibility of failure initiated by this phenomenon.

In developing an effective optimization strategy, a reliable means of detecting secondary instabilities, needs to be used. There are various approaches to detecting the onset of a structural instability in finite element analysis. Linear eigenvalue analysis, as the name suggests, is only applicable to structures which exhibit prebuckling linear behavior, are not imperfection sensitive and tend to display stable symmetric initial buckling behavior [8]. While most aero-structural components would fit this category, this type of analysis does not yield any quantitative information on the postbuckled deformation. Moreover, eigenvalue analysis may give information on the mode shape of secondary (and higher) instabilities but the loads at which these occur cannot be inferred from the eigenvalues. Robust nonlinear finite element analysis enables the determination of secondary instabilities and there are a number of numerical strategies designed to stabilize the solution around these critical regions. The ease at which instabilities may be detected and used as part of an optimization procedure is dependent on the information that can be extracted as part of the solution process. This is greatly facilitated if the user has direct access to the code which could be tailored to give the required output. For example, matrix inversion of the tangential stiffness matrix $\mathbf{K_t}$ is usually achieved by first decomposing the matrix into the product of a lower unit triangular matrix $\mathbf{L}$, a diagonal matrix, $\mathbf{D}$, and the transpose of $\mathbf{L}$, i.e., $\mathbf{LDL^T}$. Instabilities may be detected by changes in the signs of the diagonal entries in $\mathbf{D}$ which, in turn, imply a negative eigenvalue in $\mathbf{K_t}$. From a practical viewpoint, it is not always possible to extract such information from a commercial finite element package. To circumvent the possibility of being unable to extract information on the factored stiffness matrix directly, the method adopted in this paper is based on tracking the rate of change of out-of-plane displacements, with respect to the applied loading, at points distributed throughout the structure. This information only requires displacement information, which is a fundamental output of all finite element packages.

A blade-stiffened composite panel, previously tested in uniaxial compression until failure, exhibited secondary instabilities [3] where the skins between the stiffeners (skin bays) initially buckled into four half-waves before mode jumping to five half-waves and eventually six half-waves. The optimization methodology presented in this work, uses a flat plate which is representative of the central skin bay. The ply orientations were used as the design variables and the optimization process was subject to initial buckling load and prebuckling stiffness constraints to ensure a feasible design. Note that the prebuckling stiffness was determined from the linear portion of the load-displacement curve below the initial buckling point.

II. Blade-Stiffened Panel Skin Bay

A composite panel representing the central skin bay of a blade-stiffened panel was used to demonstrate the optimization concept. The panel was manufactured by British Aerospace (Military Division) from unidirectional prepreg T800/924C with material properties detailed in Table 1. The panel contained four blade stiffeners, secondary bonded to the skin using a film adhesive between the tapered flanges of the stiffener and the skin. The stiffeners were not equally spaced, making the central skin bay twice the width of the outer bays. The loaded edges at the ends of the panel were potted in a mixture of epoxy resin and fiberglass, before being machined flat and parallel to ensure uniform loading. The panel was tested in uniaxial compression, under displacement control until failure, in a custom built 250 ton testing machine at Imperial College London. This machine had a stiffness of 170 tons/mm and could accommodate panels up to 1.5 m long and 1.0 m wide [4]. Full details of the experimental setup and test results can be found in the paper by Falzon et al. [3]. The panel was seen to buckle into a four-half-wave mode shape before exhibiting a sudden mode jump to a five-half-wave configuration in each of the skin bays. It is because of the existence of such a secondary instability that this panel's configuration was chosen for this work. The panel's central skin bay, spanning the centerline of the two central stiffeners, was selected and modeled in the FE package ABAQUS/Standard [9]. The bay had dimensions 728 by 240 mm, and contained a total of 22 plies, with a layup of $[90/0_2/90/\pm 45/0/90/\pm 45/0]_S$.

III. Finite Element Model

The side edges of the skin bay were clamped to approximate the influence of the stiffeners in the real panel. One loaded end of the panel was fully clamped, while the opposite end allowed for in-plane movement to transmit loading under uniaxial compression. It is important to note that the developed FE model, representing only a portion of the panel, was chosen so as to obtain a computationally efficient model which still exhibited the secondary instability and associated mode jump observed in the experimentally tested blade-stiffened panel. The clamped boundary conditions acting on the side

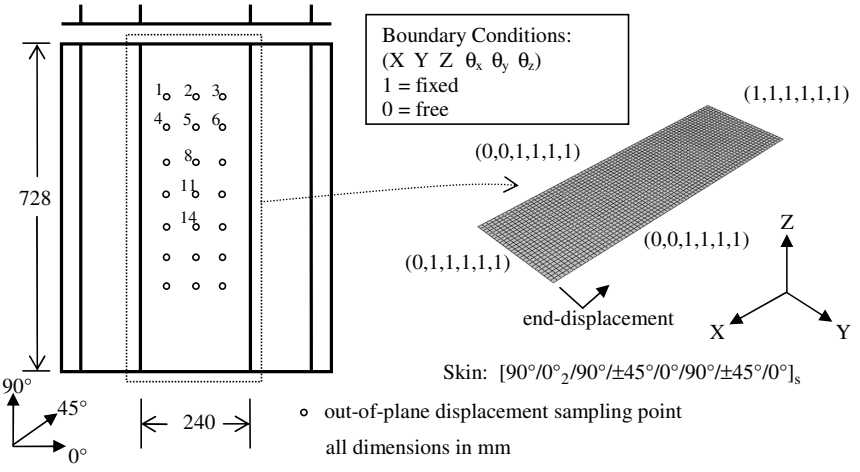

Fig. 1 FE model of central skin bay in blade-stiffened panel tested by Falzon et al. [3].

of the skin bays will only approximate the influence of the stiffeners in the full panel. In fact, the rotational restraint provided by the stiffeners is bound to be less than that imposed by a fully-clamped condition. Nonetheless, lateral clamped boundary conditions provide added lateral restraint which, in a postbuckling structure, results in high membrane stresses being generated. This restricts out-of-plane bending deformation which leads to a mode jump [21]. The model consisted of 1872 general-purpose shell elements with reduced integration (SR4), each having four nodes and six degrees of freedom at each node. Each element contained three integration points per ply through the thickness, and the skin layup of $[90/0_2/90/\pm 45/0/90/\pm 45/0]_S$ was assigned to the skin bay model. Material properties corresponding to an average of the tensile and compressive values shown in Table 1 were used. Figure 1 shows the final FE model for the skin bay and its associated mesh. Various sampling point locations on the skin bay were selected to measure out-of-plane displacements. These points, shown in Fig. 1, had a separation of 91 mm in the loading direction and 46 mm in the width direction, with point 11 corresponding to the center of the skin bay.

A linear eigenvalue buckling analysis was conducted on the skin bay in ABAQUS/Standard to find the eigenvalues and corresponding mode shapes for the skin bay loaded in uniaxial compression. A linear superposition of the first two buckle modes was then used to impose out-of-plane geometric imperfections in the skin bay model with maximum amplitude of 2% of the skin thickness, allowing a standard nonlinear quasi-static analysis to trace the full postbuckling response of the skin bay. Volume proportional damping was used in the nonlinear analysis using the ABAQUS STABILIZE parameter, which added viscous forces to the global equilibrium equations to aid convergence. Sensitivity analyses ensured that a low damping factor was used to minimize any nonrepresentative influence on the response. This value of damping corresponded to 1% of the ABAQUS default damping factor (see Sec. V).

IV. Numerical Results

Figure 2 shows the first two buckling mode shapes of four and five half-waves, respectively, which were then scaled and used as geometric imperfections for the nonlinear analysis. The nonlinear solver predicted the skin bay to buckle into a four-half-wave configuration, which correlates well with the experimentally observed Moiré fringe patterns, just after buckling, in the blade-stiffened panel's central skin bay, shown in Fig. 3a. As the skin bay model was loaded further, a secondary instability manifested itself as a sudden mode jump from the four-half-wave configuration to a five-half-wave configuration. This was consistent with experimental observations of the full stiffened panel, shown in Fig. 3b.

Figure 4a shows the numerical load-displacement curve for the skin bay, where it can be seen that at a loading of approximately 29 kN a reduction in stiffness was recorded, indicating buckling. The mode jump from four half-waves to five half-waves shows as a sudden load drop at a loading of 66.7 kN. Figure 4b shows the numerically recorded out-of-plane displacements at three locations on the skin bay. These correspond to locations 8, 11, and 14 in Fig. 1. Evidence of buckling can be seen as out-of-plane displacements start increasing rapidly, while at the onset of the secondary instability, at a loading of 66.7 kN, out-of-plane displacements show a sudden change in values. A further mode jump was also predicted at a loading of 133 kN, and this corresponded to a jump from five half-waves to six half-waves. Evidence of this mode jump is clearly visible in both the skin bay load-displacement curve and out-of-plane displacement values. It should be noted that in the preceding discussion, points 8, 11, and 14, in Fig. 4b, were selected for visualization purposes, and the selection of other locations on the panel would have been just as valid.

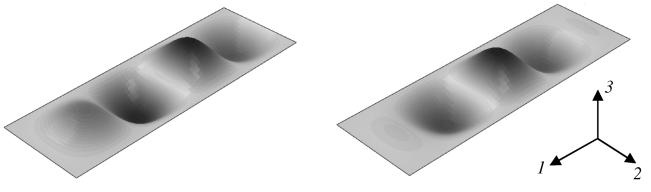

a) b)

Fig. 2 Results of an eigenvalue analysis: a) first buckling mode shape and b) second buckling mode shape.

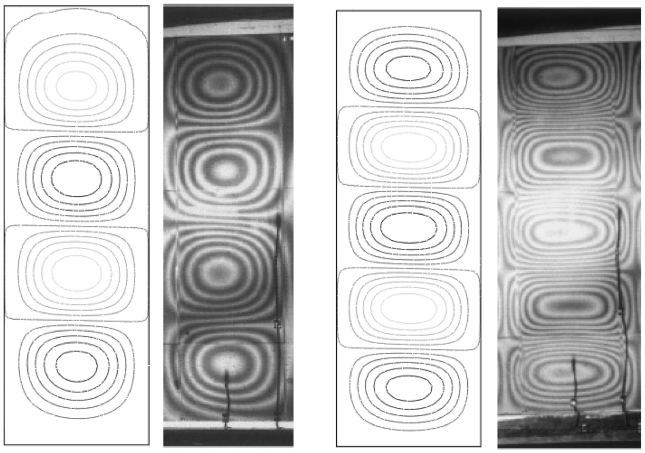

a) b)

Fig. 3 Comparison of numerically predicted out-of-plane displacement contours with experimentally observed Moiré fringe patterns in the central skin bay just after a) buckling and b) mode jump.

V. Numerical Procedure to Capture the Onset of Instabilities

The objective of the current work was to develop an optimization methodology to delay the onset of secondary instabilities. Numerical optimization techniques require repetitive function evaluations as the design variables are varied within the design space. An efficient and practical means of detecting structural instability from the displacement vector was used as part of the optimization routine.

The nonlinear FE analysis solver used to trace the postbuckling behavior of the skin bay model is based on an incremental solution scheme, where once equilibrium is established within a set tolerance at pseudotime t, a solution is sought at pseudotime $t + \Delta t$ [8]. The set of equilibrium equations to be solved are

$$\mathbf{r}^{t+\Delta t} = \lambda^{t+\Delta t}\mathbf{f}_{\text{ext}} - \mathbf{f}^{t}_{\text{int}} \tag{1}$$

where $\mathbf{r}^{t+\Delta t}$ is the residual force vector which must be below a specific tolerance for convergence, $\mathbf{f}_{\text{ext}}$ is the external reference load vector, $\lambda^{t+\Delta t}$ the load multiplier at time $t + \Delta t$, and $\mathbf{f}^{t}_{\text{int}}$ the internal force vector related to the stiffness matrix of the structure at time t. Standard nonlinear solution schemes may run into convergence difficulties in the presence of instabilities, and to stabilize the solution, pseudodamping forces $\mathbf{f}^{t+\Delta t}_{\text{damp}}$ may be applied to the equilibrium Eq. (1):

$$\mathbf{r}^{t+\Delta t} = \lambda^{t+\Delta t}\mathbf{f}_{\text{ext}} - \mathbf{f}^{t}_{\text{int}} - \mathbf{f}^{t+\Delta t}_{\text{damp}} \tag{2}$$

In the ABAQUS nonlinear solver, these damping forces are given by

$$\mathbf{f}^{\,t+\Delta t}_{\text{damp}} = c\mathbf{M}\frac{\Delta \mathbf{u}^{t+\Delta t}}{\Delta t} \tag{3}$$

Where c is a damping factor and $\mathbf{M}$ a consistent mass matrix with unit density. At the onset of an instability, out-of-plane nodal pseudovelocities $(\Delta u_3^{t+\Delta t}/\Delta t)_k$, will increase dramatically, and hence so will the damping forces in this direction.

A similar measure was used to detect both buckling and mode jumps. A series of sampling points were selected on the skin bay of the FE model, as shown in Fig. 1. Throughout the nonlinear analysis, the change in out-of-plane displacements values at these sampling

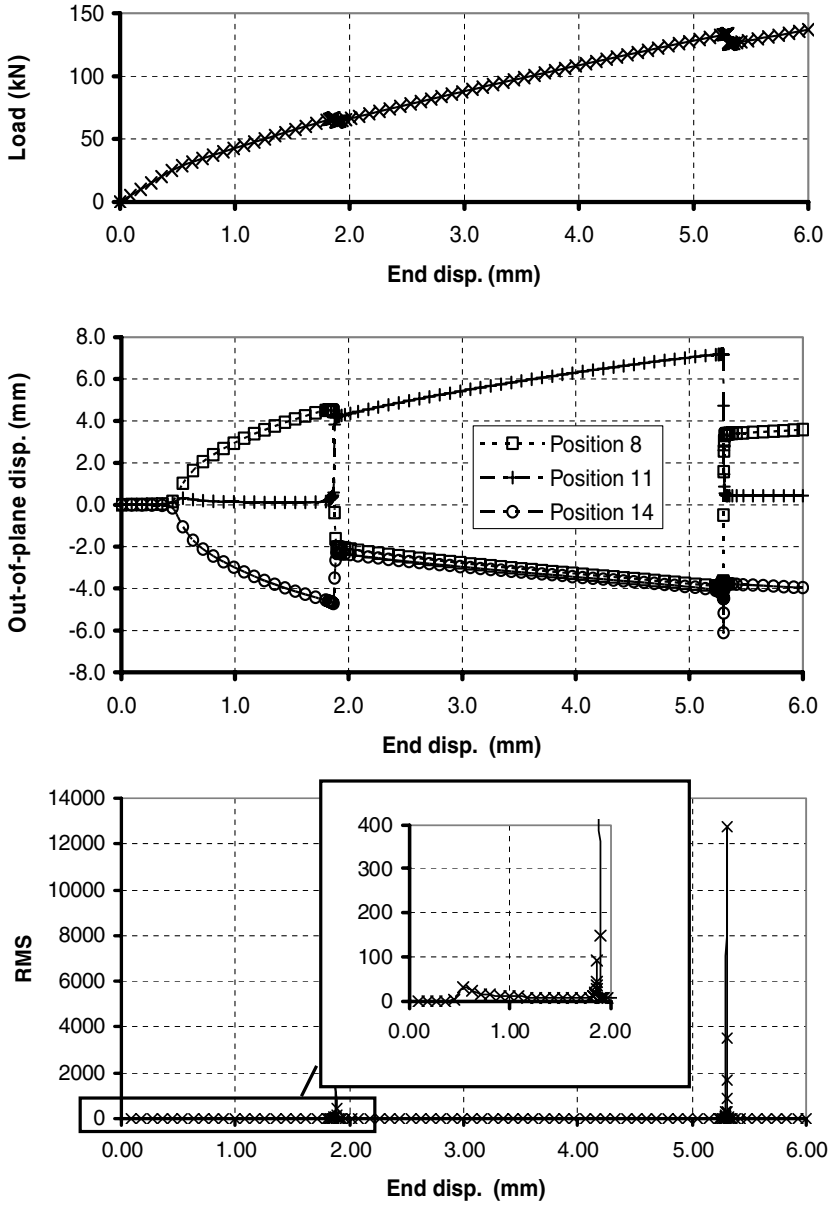

Fig. 4 FE skin bay model results: a) load against end displacement curve, b) out-of-plane displacements, and c) RMS function of Eq. (4).

points was recorded to obtain a measure of $(\Delta u_3^{t+\Delta t})/\Delta t$ for each point at each increment. The root mean square (RMS) of all values was then calculated to obtain a representative metric to indicate a structural instability:

$$\text{RMS}^{\,t+\Delta t} = \sqrt{\frac{\sum_{k=1}^{n}\left(\frac{\Delta u_3^{t+\Delta t}}{\Delta t}\right)}{n}} \tag{4}$$

where n is the number of sampling points used. A plot of $\text{RMS}^{t+\Delta t}$ function for the developed skin bay FE model is given in Fig. 4c, and shows that local maxima in the function occurred at the onset of the instabilities. A first local maximum could be seen at the buckling point. A much larger increase in the RMS metric occurred at the onset of the secondary instability associated with the mode jump from four half-waves to five half-waves, shown by the second local maximum in the RMS curve.

VI. Optimization Genetic Algorithm

A. Formulation of the Optimization Problem

The objective of the optimization procedure was to delay the onset of secondary instabilities which occurred in the skin bay as it was loaded beyond initial buckling. Evidence that secondary instabilities may cause structural failure in composite stiffened panels was first suggested by Romeo and Frulla [22] and Bushnell et al. [23]. The blade-stiffened panel used in this study was actually one of two identical panels which were tested to failure [3]. The first panel buckled at 110 kN and failed at 573 kN. The second panel, used in this paper, buckled at 105 kN and mode jumped at 570 kN before failing at 601 kN. This suggests the possibility of the first panel failing by mode jumping. More direct evidence was published by Falzon and Cerini [2] in their study of the failure of a hat-stiffened panel where experimental observations were supported by numerical modeling. In [7] it was also shown that optimizing to delay the onset of damage at the skin-stiffener interface resulted in a panel with delayed mode jumping.

During the optimization process, each different design, corresponding to a specific layup, was evaluated by means of a FE analysis and calculation of the RMS function to detect the occurrence of any secondary instability and the loading at which such instability occurred. A natural choice for the objective function was the load at which a secondary instability was observed to occur during a design's postbuckling response. The design variables for the optimization were the ply orientations of the plies in the skin bay, which were allowed to take values of 0, 45, −45, and 90°, commonly

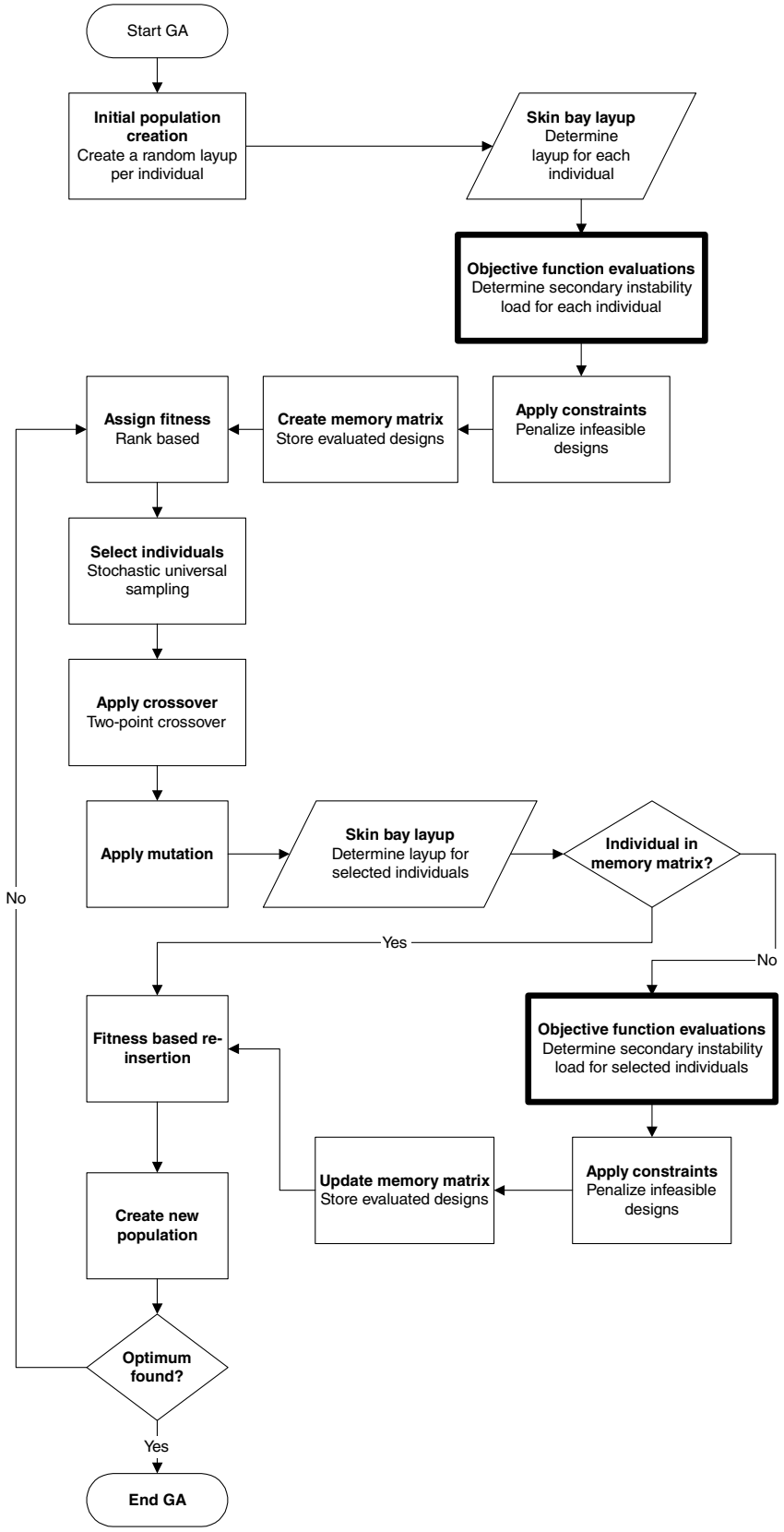

Fig. 5 Flowchart of developed GA for optimization of blade-stiffened panel skin bay to delay the onset of secondary instabilities.

used in industry. This transformed the optimization problem into a nonlinear integer programming problem with a design space of over four million possibilities, since half of the skin bay's 22 plies were considered for optimization to ensure symmetric layups. Altering the layup of the skin bay changes both its buckling as well as its postbuckling characteristics, so constraints were introduced on the prebuckling stiffness and buckling load of the skin bay to guarantee a realistic and feasible optimized design. Constraints were set by penalizing those designs which had a buckling load or prebuckling stiffness 10% less than that of the original baseline skin bay. An

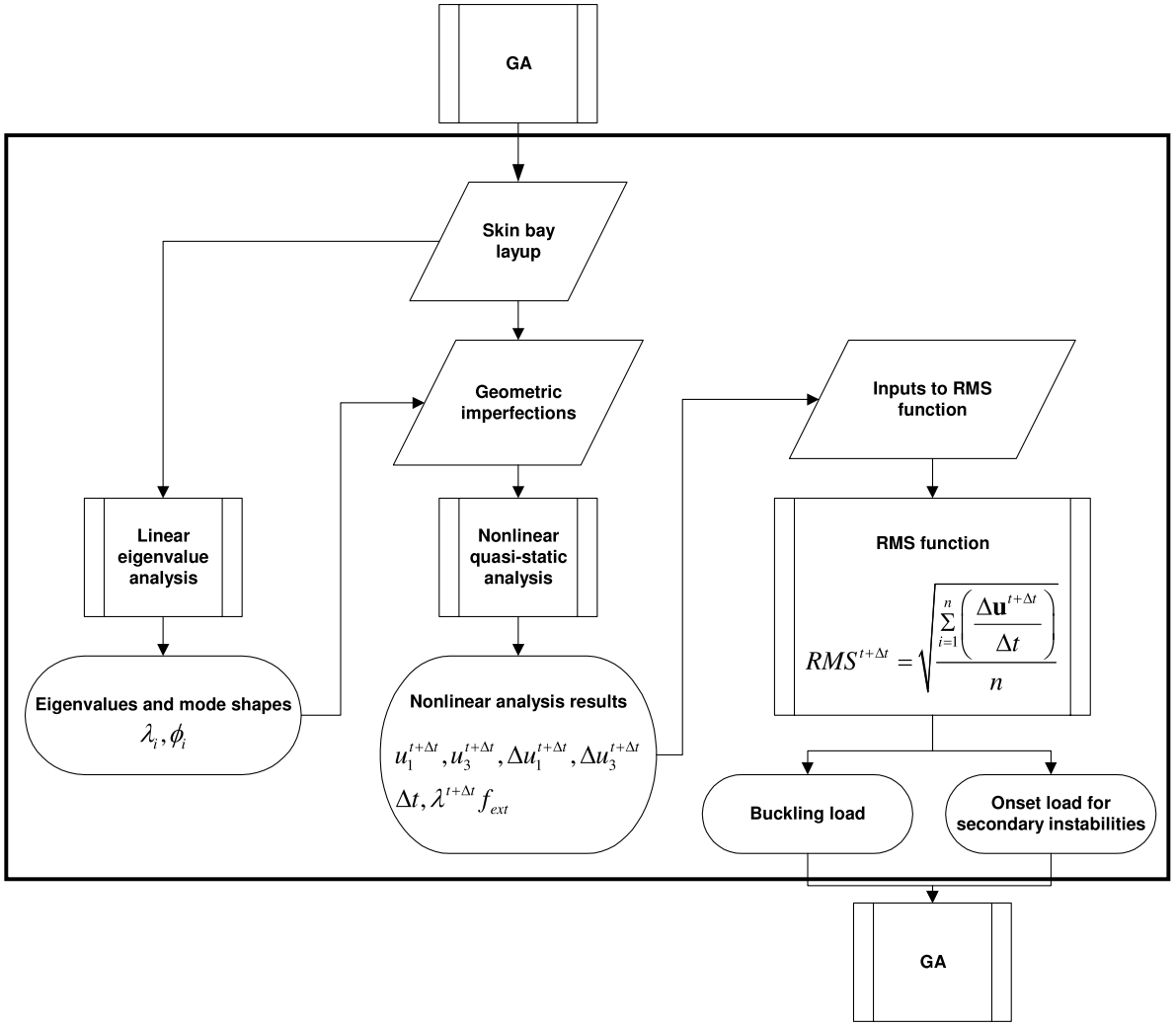

Fig. 6 Flowchart showing interaction of the GA with the FE model within the objective function evaluation module.

additional constraint was set to prevent individuals from having more than two contiguous plies in the same orientation as this can potentially promote matrix cracking [24].

Having defined the design variables, objective function, and constraints, an optimization strategy was formulated to find the layup of the skin bay to delay the onset of secondary instabilities. Ply-orientation identity variables were used [25] and each of these variables represented one of the possible ply orientations and assumed a value of one, if such ply orientation was active, and a value of zero otherwise. Plies were numbered using the index i, which took the values of $i = 1, \ldots 11$ representing the 11 plies of the skin bay half-layup.

B. Initial Population

A GA was developed in MATLAB [26] to conduct the optimization problem, and a schematic of its various operations are shown in Fig. 5. A fixed population size of 60 individuals was used, with each generation being represented by a matrix. Each row, referred to as a "chromosome string," represented an individual design. The initial population was created randomly, with each bit in the chromosome string assuming an integer value in the range one to four for each allowed ply orientation.

C. Function Evaluations

Figure 5 shows how each individual was evaluated in terms of the objective function. For each individual with a different skin bay layup, FE analyses needed to be conducted. In terms of the optimization algorithm, such function evaluations may be considered "black box" operations. In each black box, each individual was evaluated via a series of FE analyses and the use of the RMS function, as shown in Fig. 6. The layup of the skin bay was used to first run a linear eigenvalue analysis on the FE model, to reveal the eigenvalues and associate mode shapes, which where then used as geometric imperfections for the nonlinear analysis. Routines were set up to automatically extract displacement results from the ABAQUS analysis at each increment to calculate $(\Delta u_3^{t+\Delta t})/\Delta t$ for all the sampling points on the skin bay. The load at which a secondary instability occurred was then fed back to the GA, and values relating to buckling load and prebuckling stiffness were used in constraint margin calculations.

D. Constraint Penalization and Selection

Individuals violating the buckling load or prebuckling stiffness constraints were penalized. Following this, a generalized rank-based fitness scheme was used to rank all individual according to their objective function. The individual displaying the highest objective function was given a high fitness value, the worst individual a fitness of zero, and all other individuals linearly assigned values in between.

Table 2 Two-point crossover genetic operator

Parents	Offspring
24/31141/2441	24/14332/2441
12/14332/2132	12/31141/213

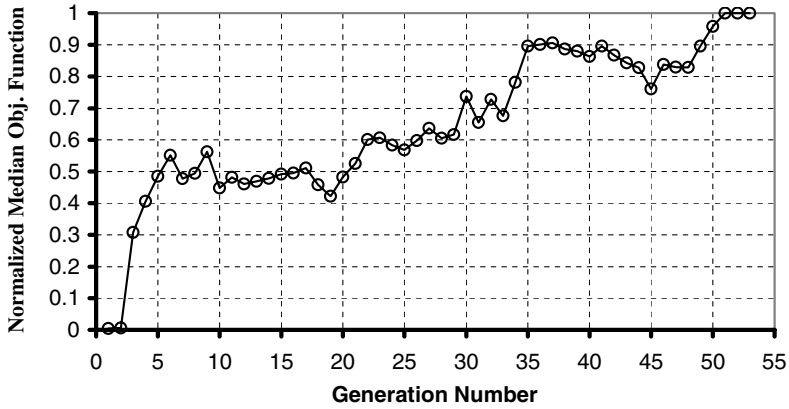

Fig. 7 Normalized median objective function plotted against GA generation number.

A fixed high value of the objective function (500) was used to guarantee that individuals not exhibiting a secondary instability remained in the gene pool. This fixed value was higher than any expected mode jump load. To distinguish between individuals which did not display secondary instabilities, the fixed value assigned to each was augmented with a value which was based on the constraint margins for stiffness and buckling load. Individuals for breeding were then selected using stochastic universal sampling [25].

E. Genetic Operators

Following selection of individuals for breeding, two-point crossover was used to create new offspring. This was done by selecting two random cutoff points in the 11-bit string and then swapping genetic information amongst the parent individuals. An example is shown in Table 2. Following crossover, mutation was applied to prevent the loss of potentially favorable genetic traits. This mutation was assigned a very low probability of occurring. Mutation acts by changing a random bit in a string and thus acts as a safety net to recover good genetic material which may have been lost during selection and crossover. Following mutation, a fitness based reinsertion scheme was used so that the generated offspring directly replaced the least fit individuals in the population. This method tends to preserve attractive genetic traits, hence aiding in achieving convergence in a reduced number of generations. The whole genetic process was repeated until the GA found the optimum layup for the skin bay to delay the onset of secondary instabilities. A termination scheme was applied so that if five successive individuals in the population had the same chromosome string, then this chromosome string was deemed as the optimum. As a safety measure, a maximum number of 100 generations was also set.

F. Memory Capability

To reduce computational cost, a memory capability was implemented in the GA. To do this, all evaluated individuals were stored in a "memory" array together with their objective function values. Before any function evaluation, this array was scanned such that if an individual had already been previously evaluated, the value of its objective function was copied rather than reevaluated using a new FE analysis. This reduced computational cost considerably, especially in the latter stages of the optimization where most individuals had already been previously evaluated in the solution history.

VII. Genetic Algorithm Results

A. Genetic Algorithm Convergence

Execution of the GA in order to find a revised skin bay layup with delayed secondary instabilities led to convergence after 53 generations. Figure 7 shows a plot of the normalized median objective function for each population against the number of generations. The initial randomly created population contained many individuals with a low objective function, but as the GA evolved, driving individuals towards the optimum, the average normalized median of the objective function increased from generation to generation. At convergence most individuals in the population had the optimal layup and highest objective function value.

B. Optimized Design

The GA identified the optimum skin bay layup to be $[0/90/-45/90/45/90_2/-45/90/-45/90]_S$. Table 3 compares

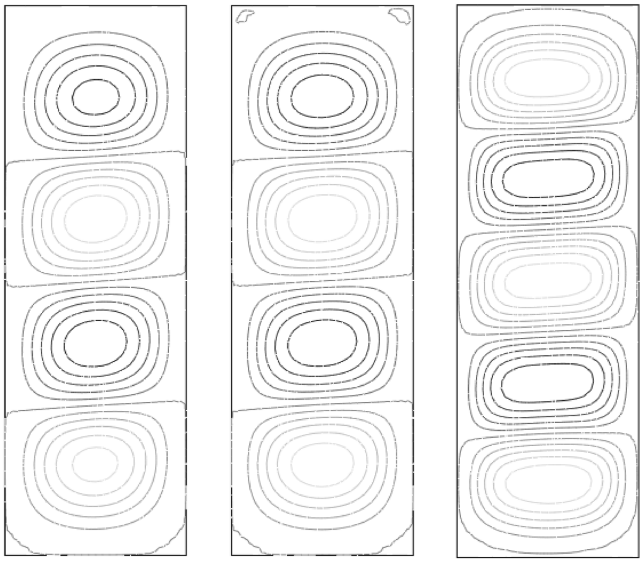

a) b) c)

Fig. 8 Numerically predicted out-of-plane displacement contours for optimized skin bay layup: a) just after buckling, b) at a loading of 66.7 kN, and c) after mode jump at 108.6 kN.

Table 3 Optimization results

Load	Nonoptimized	Optimized	Percent difference
Panel layup	$[90/0_2/90/\pm 45/0/90/\pm 45/0]_S$	$[0/90/-45/90/45/90_2/-45/90/-45/90]_S$	——
Buckling load, kN	29.2	32.3	+10.6%
Prebuckling stiffness, kN/mm	56.2	89.3	+58.9%
Onset of secondary instability, kN	66.7	119.8	+79.6%

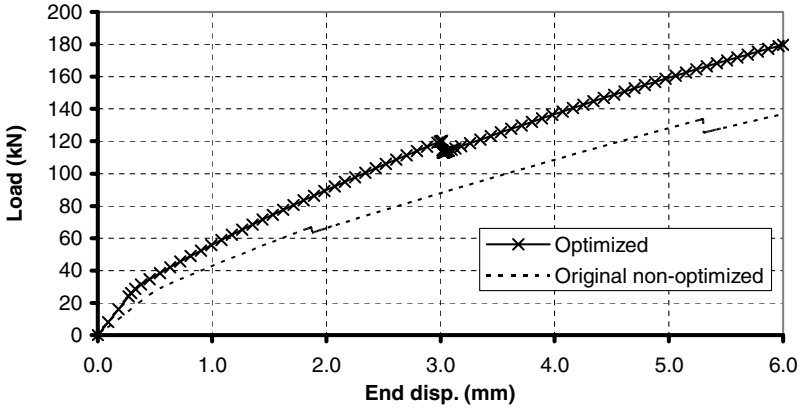

Fig. 9 Comparison of load-displacement curves for optimized and nonoptimized FE blade-stiffened panel skin bay models.

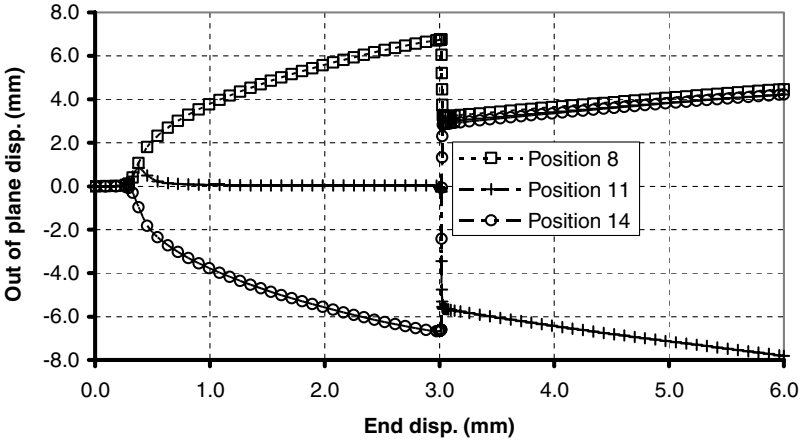

Fig. 10 Numerically predicted out-of-plane displacements in optimized FE blade-stiffened panel skin bay model.

the optimum configuration with the original, baseline skin bay layup. A linear buckling analysis predicted a buckling load for the optimized skin bay layup of 32.3 kN, 10.6% higher than the 29.2 kN value for the original baseline design. The prebuckling stiffness of the optimum design was 89.3 kN, 58.9% higher than that of the nonoptimized design. The GA was hence able to find an optimum solution not only within the bounds of the constraints imposed on the optimization—a maximum of 10% reduction in buckling load and prebuckling stiffness as compared with the original baseline skin bay model, but in fact yielded an optimum design with superior buckling load and stiffness where a secondary instability was delayed to occur at a load of 119.8 kN compared with the nonoptimized value of 66.7 kN.

The mode shapes corresponding to the first two eigenvalues for the optimized skin bay were very similar to those of the nonoptimized skin bay shown in Fig. 2. The behavior of the optimized skin bay model, as predicted by the ABAQUS nonlinear solver, is shown in Fig. 8 in terms of out-of-plane displacement contours, which may be compared with Fig. 3 for the nonoptimized skin bay. Similarly to the nonoptimized skin bay, the optimized design buckled into a four-half-wave configuration as shown in Fig. 8a, but at the higher buckling load of 32.3 kN, compared with 29.2 kN. As the loading was increased, the nonoptimized skin bay mode jumped to a five-half-wave configuration at a loading of 66.7 kN, while the optimized skin bay maintained its four-half-wave configuration, shown in Fig. 8b. A secondary instability in the optimized skin bay developed at the higher loading of 119.8 kN, also corresponding to a sudden mode jump from four to five half-wavelengths, shown in Fig. 8c.

Figure 9 shows the load-displacement curve for the optimal skin bay layup. The load-displacement curve of the original panel as in Fig. 4a is also shown for comparative purposes. It can be seen that the optimized design shows a greater buckling load and prebuckling stiffness, and evidence of the mode jump from four to five half-waves can be seen as a slight load drop in the load-displacement curve which occurs at a substantially higher loading for the optimized configuration. Figure 10 shows numerically recorded out-of-plane displacements at the same positions on the skin bay as was shown in Fig. 4b for the nonoptimized panel. The occurrence of buckling is marked by a rapid increase in out-of-plane displacement values, and evidence of a secondary instability and associated mode jump is clearly visible via the sudden change in out-of-plane displacement measurements as was discussed for the case of the nonoptimized skin bay.

VIII. Conclusions

A simple and computationally efficient numerical routine was used to detect structural instabilities in a compressively loaded composite structure. The routine extracted the rate of change of out-of-plane displacement values from the finite element model at various sampling points which were then used to detect the onset of structural instability. An optimization routine was developed which made use of this metric to optimize the layup of the composite structure to delay the onset of secondary instabilities.

As a proof of concept of the developed methodology, a representative section, corresponding to the skin bay of a blade-stiffened composite panel was modeled. This skin bay, with clamped boundary conditions and loaded in uniaxial compression, buckled into a four-half-wave configuration followed by a sudden mode jump to a five-half-wave configuration, matching the behavior observed in the experimental testing of the complete blade-stiffened panel. The optimization routine was applied to the skin bay model and was able to effectively delay the onset of the secondary instability. Constraints

were imposed on the stiffness and buckling load of the baseline value to ensure that the optimum design was still feasible.

The developed methodology is readily applicable to more complex composite structures. The same numerical routine could be used to detect buckling and secondary instabilities and linked to the GA to perform an optimization subject to user-defined constraints. Experimental evidence points to the possibility of secondary instabilities in composite structures causing structural failure by promoting skin-stiffener debonding which can ultimately lead to catastrophic collapse. Hence a method of delaying such instabilities may considerably improve the postbuckling performance of composite structures.

References

[1] Falzon, B. G., "The Behaviour of Damage Tolerant Hat-Stiffened Composite Panels Loaded in Uniaxial Compression," *Composites, Part A: Applied Science and Manufacturing*, Vol. 32, No. 9, 2001, pp. 1255–1262.
doi:10.1016/S1359-835X(01)00074-4

[2] Falzon, B. G., and Cerini, M., "A Study of Secondary Instabilities in Postbuckling Composite Aerostructures," *Aeronautical Journal*, Vol. 111, No. 1125, Nov. 2007, pp. 715–729.

[3] Falzon, B. G., Stevens, K. A., and Davies, G. A. O., "Postbuckling Behaviour of a Bladehyphstiffened Composite Panel Loaded in Uniaxial Compression," *Composites, Part A: Applied Science and Manufacturing*, Vol. 31, No. 5, 2000, pp. 459–468.
doi:10.1016/S1359-835X(99)00085-8

[4] Singer, J., Arborcz, J., and Weller, T., *Buckling Experiments*, Vol. 1, Wiley, New York, 1998.

[5] Singer, J., Arborcz, J., and Weller, T., *Buckling Experiments*, Vol. 2, Wiley, New York, 2002.

[6] Bushnell, D., Rankin, C. C., and Riks, E., "Optimization of Stiffened Panels in Which Mode Jumping is Accounted For," *38th AIAA/ASME/ASCE/AHS/ASC Structures, Structural Dynamics and Materials Conference*, Kissimee, FL, 1997, pp. 2124–2162.

[7] Faggiani, A., and Falzon, B. G., "Optimization Strategy for Minimizing Damage in Postbuckling Stiffened Panels," *AIAA Journal*, Vol. 45, No. 10, 2007, pp. 2520–2528.
doi:10.2514/1.26910

[8] Falzon, B. G., and Hitchings, D., *An Introduction to Buckling and Collapse*, 2nd ed., NAFEMS, Glasgow, Scotland, 2007.

[9] ABAQUS Ver. 6.8, Dessault Systems, Providence, RI, 2008.

[10] Holland, J. H., *Adaptation in Natural and Artificial Systems*, Univ. of Michigan Press, Ann Arbor, MI, 1975.

[11] Le Riche, R., and Haftka, R. T., "Optimization of Laminate Stacking Sequence for Buckling Load Maximization by Genetic Algorithm," *AIAA Journal*, Vol. 31, No. 5, 1993, pp. 951–970.
doi:10.2514/3.11710

[12] Le Riche, R., and Haftka, R. T., "Improved Genetic Algorithm for Minimum Thickness Composite Laminate Design," *Composites Engineering*, Vol. 5, No. 2, 1995, pp. 143–161.
doi:10.1016/0961-9526(95)90710-S

[13] Kogiso, N., Watson, L. T., Gurdal, Z., Hafta, R. T., and Nagendra, S., "Minimum Thickness Design of Composite Laminates Subject to Buckling and Strength Constraints by Genetic Algorithm," AIAA/ASME/ASCE/AHS/ASC Structures, Structural Dynamics and Materials Conference, Hilton Head, SC, AIAA Paper 94-1600-CP, April 1994.

[14] Nagendra, S., Jestin, D., Gurdal, Z., Hafta, R. T., and Watson, L. T., "Improved Genetic Algorithm for the Design of Stiffened Composite Panels," *Computers and Structures*, Vol. 58, No. 3, 1996, pp. 543–555.
doi:10.1016/0045-7949(95)00160-I

[15] Gantovnik, V. B., Anderson-Cook, C. M., Gurdal, Z., and Watson, L. T., "A Genetic Algorithm with Memory for Mixed Discrete-Continuous Design Optimization," *Computers and Structures*, Vol. 81, No. 20, 2003, pp. 2003–2009.
doi:10.1016/S0045-7949(03)00253-0

[16] Gantovnik, V. B., Gurdal, Z., and Watson, L. T., "A Genetic Algorithm with Memory for Optimal Design of Laminated Sandwich Composite Panels," *Composite Structures*, Vol. 58, No. 4, 2002, pp. 513–520.
doi:10.1016/S0263-8223(02)00128-9

[17] Di Sciuva, M., Gherlone, M., and Lomario, D., "Multiconstrained Optimization of Laminated and Sandwich Plates Using Evolutionary Algorithms and Higher-Order Plate Theories," *Composite Structures*, Vol. 59, No. 1, 2003, pp. 149–154.
doi:10.1016/S0263-8223(02)00132-0

[18] Bisagni, C., and Lanzi, L., "Post-Buckling Optimization of Composite Stiffened Panels Using Neural Networks," *Composite Structures*, Vol. 58, No. 2, 2002, pp. 237–247.
doi:10.1016/S0263-8223(02)00053-3

[19] Lanzi, L., and Bisagni, C., "Minimum Weight Optimization of Composite Stiffened Panels Using Neural Networks," 44th AIAA/ASME/ASCEAHS Structures, Structural Dynamics, and Materials Conference, Norfolk, VA, AIAA Paper 2003-1698, 2003.

[20] Lanzi, L., "Multi-Objective Optimization of Composite Stiffened Panels: Computations and Experiments," *Computational and Experimental Engineering and Science*, Tech Science, Madeira, Portugal, 2004.

[21] Koiter, W. T., "Introduction to the Post-Buckling Behaviour of Flat Plates," *Colloquium on the Post-Buckling Behaviour of Plates in Metal Structures*, Univ. of Liege, Liege, Belgium, The Netherlands, 1963.

[22] Romeo, G., and Frulla, G., "Nonlinear Analysis of Anisotropic Plates with Initial Imperfections and Various Boundary Conditions Subjected to Combined Biaxial Compression and Shear Loads," *International Journal of Solids and Structures*, Vol. 31, No. 6, 1994, pp. 763–783.
doi:10.1016/0020-7683(94)90076-0

[23] Bushnell, D., Rankin, C. C., and Riks, E., "Optimization of Stiffened Panels in Which Mode Jumping is Accounted For," 38th AIAA/ASME/ASCE/AHS/ASC Structures, Structural Dynamics and Materials Conference, Kissimmee, FL, 1997.

[24] Haftka, R. T., and Walsh, J. L., "Stacking-Sequence Optimization for Buckling of Laminated Plates by Integer Programming," *AIAA Journal*, Vol. 30, No. 3, 1992, pp. 814–819.
doi:10.2514/3.10989

[25] Gurdal, Z., Hafta, R. T., and Hajela, P., *Design and Optimization of Laminated Composite Materials*, Wiley, New York, 1999.

[26] MATLAB, Mathworks, Natick, MA, 2009.

S. Pellegrino
Associate Editor